Journal of Materials Chemistry

Cite this: J. Mater. Chem., 2012, 22, 20535

www.rsc.org/materials

PAPER

A combined first principles and experimental study on $Na_3V_2(PO_4)_2F_3$ for rechargeable Na batteries†

R. A. Shakoor,‡[a] Dong-Hwa Seo,‡[b] Hyungsub Kim,[bc] Young-Uk Park,[b] Jongsoon Kim,[b] Sung-Wook Kim,[b] Hyeokjo Gwon,[a] Seongsu Lee[c] and Kisuk Kang*[b]

Received 15th June 2012, Accepted 9th August 2012
DOI: 10.1039/c2jm33862a

The electrochemical properties of $Na_3V_2(PO_4)_2F_3$ in a Na rechargeable battery were investigated through a combined computational and experimental study. *Ex situ* XRD results indicate that the reversible sodiation/desodiation occurs *via* one phase reaction and the structure of $Na_{3-x}V_2(PO_4)_2F_3$ remains quite stable upon extraction and insertion of sodium. Notable is that the one phase reaction is accompanied by the negligible variation in lattice parameters (~1%) and unit cell volume (~2%) which results in a good cycle performance. It is further noticed that the desodiated phase is thermally stable up to 550 °C implying the excellent safety characteristic of the charged electrode. The first principles calculations elucidate the mechanisms of the structural evolution and the electrochemical behavior of $Na_{3-x}V_2(PO_4)_2F_3$ upon battery cycling.

Introduction

The environmental pollution and gradual depletion of oil resources have gained much attention in recent years. In order to overcome these issues, a considerable development has been made in the area of energy storage system including lithium batteries. However, it is pertinent that if a new energy economy is to appear, it should be cheap and sustainable. A close assessment of lithium reserves vital to the lithium battery chemistry reveals that most of the untapped reserves are located in politically sensitive areas.[1,2] Therefore, keeping in view the sustainability and economy, the development of resources as alternatives to lithium may be of importance.[3–7] Recently, the Na-ion batteries have been considered as an attractive alternative to Li-ion batteries due to reasons such as: (i) good economic efficiency, (ii) rich resources of sodium, (iii) lower material costs, (iv) low toxicity, and (v) ability to utilize electrolytes at low decomposition potential.[3,8] In addition, we can take advantage of the well-established understanding of the lithium based electrochemical system for the development of Na (or a similar alkali atom) counterpart. Although sodium batteries may offer significant advantages, they have been little studied compared with lithium batteries.[3,9] This may be due to the great success of Li ion batteries that has suppressed this important area for many years.[1,10–13]

In recent years, the fluorophosphates having a NASICON (Na Super-Ionic Conductor) type structure have been proposed as an electrode material for electrochemical systems.[4,14–21] These fluorophosphates exhibit rich chemistry, attractive lithium/sodium insertion properties and thus offer promising electrochemical properties. Among them, $Na_3V_2(PO_4)_2F_3$ deserves attention because of promising electrochemical properties and ease of fabrication. Meins *et al.* first reported the crystal structure of $Na_3V_2(PO_4)_2F_3$ with the space group of $P4_2/mnm$.[22] Gover *et al.* reported its electrochemical behavior such as the high specific capacity (~120 mA h g^{-1}), high discharge voltage (~4.1 V *vs.* Li^+/Li^0) and good cyclability in a lithium cell.[17] Barker *et al.* reported the electrochemical performance of $Na_3V_2(PO_4)_2F_3$ in a graphite/Li^+ electrolyte/$Na_3V_2(PO_4)_2F_3$ hybrid cell.[18] They demonstrated that $Na_3V_2(PO_4)_2F_3$ can be a potential cathode material in the conventional lithium cell. Recently, Jiang *et al.* proposed a simple sol–gel process to prepare $Na_3V_2(PO_4)_2F_3$/carbon.[21] They demonstrated that this composite structure showed good charge/discharge capacity (127 mA h g^{-1}) and good cyclability. The promising electrochemical properties of this composite structure were attributed to the improvement in electrical conductivity due to the presence of carbon, its inherent open NASICON structure and its structural stability during insertion/de-insertion of lithium. Although a few studies are available on the structure and electrochemical properties of $Na_3V_2(PO_4)_2F_3$ in a lithium cell, nevertheless, the detailed electrochemical behavior of $Na_3V_2(PO_4)_2F_3$ has not been investigated thoroughly. Since the studies on the crystal and electronic structure of the electrode material are crucial in improving the

[a]*Department of Materials Science and Engineering, KAIST, 291 Daehak-ro, Yuseong-gu, Daejeon 305-701, Republic of Korea*
[b]*Department of Materials Science and Engineering, Research Institute of Advanced Materials, Seoul National University, 599 Gwanak-ro, Gwanak-gu, Seoul 151-742, Republic of Korea. E-mail: matlgen1@snu.ac.kr; Fax: +82 2 880 8197; Tel: +82 2 880 7165*
[c]*Korea Atomic Energy Research Institute, P.O. Box 105, Yuseong-gu, Daejeon 305-600, Republic of Korea*
† Electronic supplementary information (ESI) available: SEM image of $Na_3V_2(PO_4)_2F_3$. See DOI: 10.1039/c2jm33862a
‡ These two authors contributed equally.

electrochemical performance, in the present work, a combined first principles and experimental investigation on $Na_3V_2(PO_4)_2F_3$ has been undertaken to reveal its structural evolution associated with the Na ion insertion/extraction and electrochemical properties in a sodium cell. Furthermore, the study of $Na_3V_2(PO_4)_2F_3$ in a sodium cell will also assist in understanding its promising electrochemical properties and employing $Na_3V_2(PO_4)_2F_3$ as a potential cathode for high performance sodium batteries.

Experimental section

Material synthesis

$Na_3V_2(PO_4)_2F_3$ was prepared by a two-step reaction as proposed in previous work[18] under slightly modified reaction conditions. In the first step, VPO_4 was synthesized by reacting stoichiometric amounts of $NH_4H_2PO_4$ (Extra pure, JUNSEI), V_2O_5 (99.9%, SMC) and carbon black (Super-P, TIMCAL). More precisely, in one typical batch, the precursors of V_2O_5 (9.0494 g), $NH_4H_2PO_4$ (11.503 g) and carbon black (1.2 g) were taken. The powders were intimately mixed for 24 hours through a dry ball milling process at a speed of 190–200 rpm and then pelletized. The pellets were sintered at 750 °C for 4 hours in the presence of flowing argon gas. The pellets were cooled to room temperature and ground, which resulted in a dark black powder. In the second step, the stoichiometric amounts of VPO_4 (prepared in the first step) and NaF (+99%, Aldrich) were intimately mixed. In one typical batch, the precursors of VPO_4 (3.6478 g) and NaF (1.04975 g) were taken. The mixture was pelletized. The pellets were then sintered at 750 °C for 1.5 hours in the presence of flowing argon gas to obtain the pure phase. When cooled to room temperature, black colored powders were thus obtained according to the following chemical reaction. The residual carbon content after the heat treatment was ~5 wt%.

$$2VPO_4 + 3NaF \rightarrow Na_3V_2(PO_4)_2F_3$$

Material characterization

The phase purity and crystal structure of synthesized materials were evaluated with an X-ray Diffractometer (Rigaku, D/MAX-RB diffractometer, Tokyo, Japan) equipped with Cu Kα radiation. The Neutron diffraction analysis of $Na_3V_2(PO_4)_2F_3$ was also performed to obtain accurate structural information and sodium occupancies. The Neutron diffraction data were recorded over the 2θ range of 0° to 160° with a step size of 0.05° with $\lambda =$ 1.8348 Å supplied by a Ge (331) single crystal monochromator on a High-Resolution Powder Diffractometer (HRPD) at the HANARO facility at the Korea Atomic Energy Research Institute. The diffraction data were refined by Rietveld refinement using FullProf Software.[23] *Ex situ* X-ray diffraction (XRD) analyses were performed at various points during charging and discharging in a voltage window of 4.5 V and 2.0 V, respectively. Upon reaching the desired cut off voltage, the potential was on hold for 2 h to ensure the equilibrium states of the electrodes. Then, the cells were disassembled inside an argon filled glove box. Next, the disassembled electrodes were thoroughly washed with propylene carbonate (PC) and dried at room temperature for 24 h inside the glove box. The XRD patterns were recorded under ambient conditions at a scan speed of 1° min^{-1} with a step size of 0.01°. The voltage and current for the XRD characterization were 40 kV and 300 mA, respectively. The size and morphology of powder particles were determined using a field emission scanning electron microscope (FE-SEM, Philips, XL30 FEG, Eindhoven, Netherlands). The compositional analysis of the synthesized material was carried out by inductively coupled plasma atomic emission spectroscopy (ICP-AES, Thermo Jarrel Ash, Polyscan 60E, U.S). The ICP composition analysis of the pristine sample confirmed the Na/V ratio was close to the target value, 1.57. Thermal stability of the chemically desodiated phase was studied by TGA/DTA using a Setsys 16/18 thermo gravimetry analyzer (SETARAM, France). The TGA/DTA data were recorded from room temperature to 500 °C at a heating rate of 10 °C min^{-1} under nitrogen atmosphere. The carbon content was measured with a carbon–sulfur determinator (CS-800; ELTRA, Germany).

Electrochemical characterization

The synthesized powder of $Na_3V_2(PO_4)_2F_3$ (containing ~5 wt% residual carbon) was coated with carbon through a dry ball milling process to improve the electrical conductivity. The mixing ratio was adjusted to make a mixture of 80 wt% active material and 20 wt% carbon (Super-P, TIMCAL). They were thoroughly mixed for 24 hours using a planetary ball mill at a speed of 320 rpm. The electrode was prepared by mixing the active material (the carbon coated $Na_3V_2(PO_4)_2F_3$), carbon black (Super-P, TIMCAL) and polyvinylidene fluoride (PVDF) in a weight ratio of 75%, 15%, 10%, respectively, which resulted in 60 wt% active material, 30 wt% total carbon, and 10 wt% PVDF. The slurry of the mixture was made by adding an appropriate amount of *N*-methyl-2-pyrrolidone (NMP) and cast on an aluminum foil using a doctor blade. The NMP was evaporated at 110 °C for 2 hours followed by punching of electrodes to the desired size. The average mass loading of the active material on the electrode was 1.85 mg cm^{-2}. All of the specific capacities were calculated based on the mass of active material. The Swagelok cells were assembled in an argon-filled glove box using a disk of sodium metal as a counter electrode and 1 M $NaClO_4$ solution in PC as an electrolyte. The electrochemical properties were studied with a battery cycler (WonA Tech, WBCS 3000, Korea) in the range of 2.0–4.5 V at various *C*-rates. For galvanostatic charge/discharge tests, the current rate was *C*/10 (12.82 mA g^{-1}) for both charge and discharge. 1*C* corresponds to 128.2 mA g^{-1} calculated from the theoretical capacity of $Na_3V_2(PO_4)_2F_3$ (128.2 mA h g^{-1}). For the rate capability test, all electrochemical cells were charged to 4.5 V at a rate of *C*/20, and then discharged to 2.0 V at various *C* rates. Unless otherwise noted, all voltage values were referenced to the standard redox potential of Na^+/Na^0.

Computation

All calculations on $Na_3V_2(PO_4)_2F_3$ were performed with the spin-polarized Generalized Gradient Approximation (GGA) using the Perdew–Burke–Ernzerhof (PBE) exchange-correlation parameterization to Density Functional Theory (DFT).[24] A plane wave basis set and the projector-augmented wave (PAW)

method were implemented in the Vienna *ab initio* simulation package (VASP).[25] PAW potentials have been widely used for battery materials and have shown good predictive capability.[26–36] The GGA + *U* approach was employed with the rotationally invariant scheme as presented by Liechtenstein.[37] *U* is the onsite coulomb term and *J* is the exchange term in the GGA + *U* approach. The *U* value of 5 eV and the *J* value of 1 eV were used for the d orbital of vanadium ions.[38] All calculations were conducted in a unit cell of 4 formula units of $Na_xV_2(PO_4)_2F_3$ at $x =$ 3, 2 and 1. A plane-wave basis with a kinetic energy cutoff of 500 eV was used, and appropriate *k*-point meshes were chosen to ensure that the total energies are converged within 2 meV per formula unit.

Results and discussion

Structural evolution with Na extraction and insertion

Fig. 1 illustrates the crystal structure of $Na_3V_2(PO_4)_2F_3$ projected on the *bc* plane (Fig. 1a) and *ab* plane (Fig. 1b). The framework of the crystal can be described in terms of $[V_2O_8F_3]$ bi-octahedral and $[PO_4]$ tetrahedral units. The bi-octahedra are linked by one of the fluorine atoms, whereas the oxygen atoms are all interconnected through the $[PO_4]$ units. This arrangement leads to the formation of channels along *a* and *b* directions with sodium located in the tunnel sites. The presence of channels in the structure provides apparent pathways for diffusion of Na ions.[17,20,22,38] Na ions can occupy a triangular prismatic site surrounded by two F ions and four O ions or an augmented triangular prismatic site attached to the F apex-square pyramid. These sites alternately form a circle-like geometry which is repeated in the *ab* plane as shown in Fig. 1c. The site energy of the Na ion at each site was calculated to determine the preferred occupancy of Na ions. The energies were obtained by adding one Na into each site of the desodiated phase, $NaV_2(PO_4)_2F_3$, and compared. The calculated site energy of the augmented triangular prismatic site is 56 meV lower than that of a triangular prismatic site in $NaV_2(PO_4)_2F_3$. This is probably due to a larger space of an augmented triangular prismatic site (18.588 $Å^3$) as compared to a triangular prismatic site (12.752 $Å^3$). In order to find out the ground state structure of $Na_3V_2(PO_4)_2F_3$, we have performed structural relaxation with all possible Na configurations. Among these Na configurations, the most stable Na configuration was determined and is shown in Fig. 1d. It appears that three augmented triangular prismatic sites are occupied out of 8 available Na sites. The short distance between these Na sites (2.92 Å) shifts the Na ion off the center of the augmented prismatic site towards a vacant Na site as shown in Fig. 1d. Fig. 2a and b represent the experimental X-ray diffraction (XRD) and neutron diffraction (ND) spectra of the pristine $Na_3V_2(PO_4)_2F_3$. No noticeable impurities were observed. The XRD and ND patterns were refined in a $P4_2/mnm$ space group. The refined lattice parameters are tabulated in Table 1. Lattice parameters obtained from XRD and ND are in good agreement with the DFT results and the previously reported values.[17,22] The detailed structural information with atomic positions and occupancies of elements is presented in Table 2. The refinement of the ND pattern reveals that Na preferentially occupies augmented triangular prismatic sites, which is consistent with the DFT calculation of the site energies. The refined Na configuration among four augmented triangular prismatic sites in Fig. 1b is also similar to the DFT predictions in Fig. 1d. However, two sodium sites (Na1) are fully occupied, while the other two (Na2) are half occupied by Na ions in $Na_3V_2(PO_4)_2F_3$. To distinguish site occupancies, different notations for these symmetrically same sites are used. Fully occupied Na sites are denoted as the Na1 site and the half occupied Na sites are denoted as the Na2 site in Fig. 1b. Na ions in Na1 sites slightly shift off the centers of augmented prismatic sites. The Na ion in the Na2 site shifts more to the opposite due to the repulsion with the Na ion in the neighbor Na1 site. Because the distance between nearby Na2 sites is 1.865 Å, two neighboring Na2 sites cannot be simultaneously occupied due to large electrostatic repulsions of Na–Na. The shift of the Na position in the augmented prismatic site is in good agreement with our calculated results.

The structural evolution of $Na_3V_2(PO_4)_2F_3$ upon electrochemical desodiation in the Na battery was investigated through *ex situ* XRD study. A comparison of *ex situ* XRD patterns of the

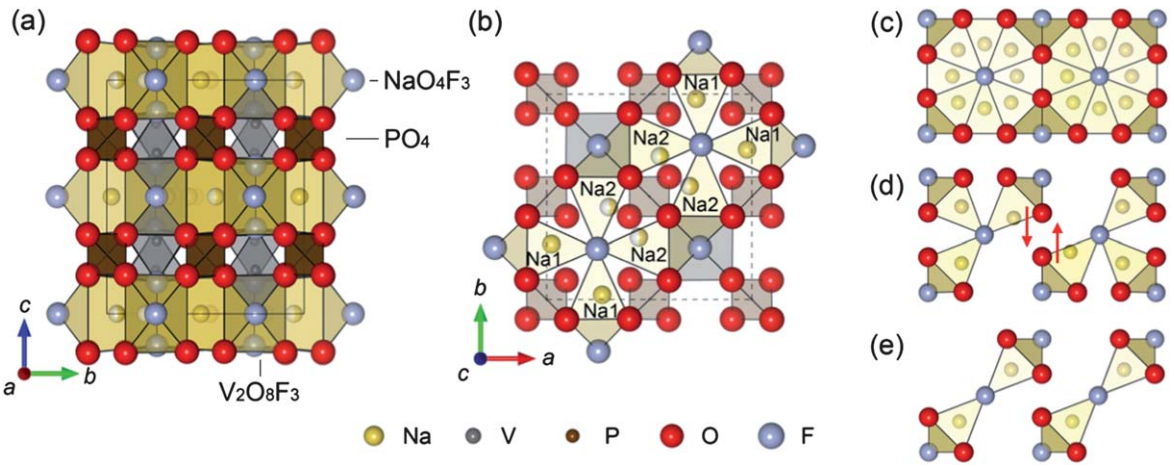

Fig. 1 Schematic representation of a refined $Na_3V_2(PO_4)_2F_3$ structure projected along (a) the *a* axis and (b) the *c* axis, (c) all of the possible Na sites and (d) most stable configuration of Na ions in $Na_3V_2(PO_4)_2F_3$ and (e) $Na_2V_2(PO_4)_2F_3$ from the first principles calculations. Na1 indicates fully occupied Na sites and Na2 indicates half occupied Na sites. Red arrows of (d) represent a shift of Na ions off the centers of prismatic sites.

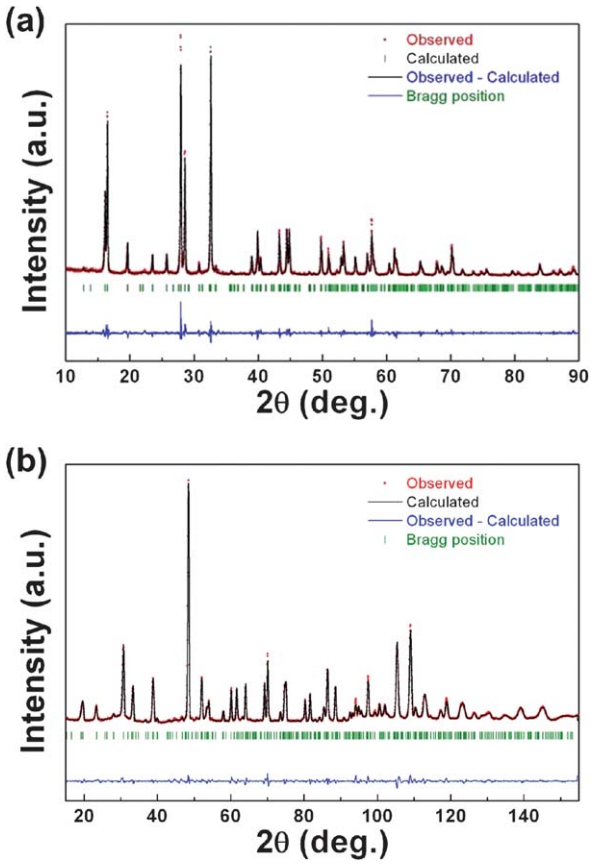

Fig. 2 (a) Rietveld refined XRD pattern and (b) Rietveld refined neutron diffraction pattern of $Na_3V_2(PO_4)_2F_3$.

$Na_3V_2(PO_4)_2F_3$ electrode at different potentials for charging and discharging is presented in Fig. 3a and b. It can be clearly noticed that the charging of the electrode up to 4.5 V shows no apparent change in diffraction patterns implying topotactic Na extraction. The main peaks at ~16° and ~28° shift continuously, reminiscent of a single-phase reaction. Table 3 shows the corresponding refined lattice parameters as a function of state of charge (SOC), suggesting that there was a linear dependence between them upon cycling. The variation in lattice parameters results in the contraction of unit cell volume by 1.79%. During the discharge, a reverse process to the charge is observed. It can be noticed that the volumetric change of $Na_3V_2(PO_4)_2F_3$ during charging and discharging is relatively small when compared to other cathode materials such as $LiFePO_4$ (6.5%), $LiMnPO_4$ (9.1%) and $LiMn_2O_4$ (6.4%) in lithium batteries even though the Na ion is bigger than the Li ion.[27,39] This small volume change may facilitate the diffusion of Na ions in the structure and cause minimal distortion of the crystal lattice. Thus, it is expected to contribute to the good cyclability and rate capability of the $Na_xV_2(PO_4)_2F_3$ electrode.

Table 1 Lattice parameters of $Na_xV_2(PO_4)_2F_3$ at $x = 3$ and $x = 1$ from XRD, ND and DFT calculations

		a (Å)	c (Å)	Volume (Å^3)
$Na_3V_2(PO_4)_2F_3$	XRD	9.04(5)	10.73(9)	876.9(4)
	ND	9.034(3)	10.740(8)	876.7(3)
	DFT	9.034	10.679	871.5
$NaV_2(PO_4)_2F_3$	XRD	8.930(2)	10.80(4)	861.2(4)
	DFT	8.863	10.772	846.2

Table 2 Refined ND data for $Na_3V_2(PO_4)_2F_3$ showing structural parameters, atomic positions of elements and occupancies

Atom	Site	x	y	z	B_{iso}	Occupancy
Na1	8	0.5252(7)	0.242(2)	0(−)	2.7 (1)	0.994(4)
Na2	8	0.837(1)	0.060(1)	0(−)	3.7(4)	0.506(4)
V1	8	0.254(5)	0.254(5)	0.193(3)	0.58	1
P1	4	0(−)	0.5(−)	0.25(−)	0.9(3)	1
P2	4	0(−)	0(−)	0.2578(9)	0.5(2)	1
O1	16	0.0983(7)	0.4073(7)	0.1694(3)	1.4(1)	1
O2	8	0.0963(6)	0.0963(6)	0.1621(6)	0.2(1)	1
O3	8	0.4044(6)	0.4044(6)	0.1565(5)	0.8(2)	1
F1	4	0.248(1)	0.248(1)	0(−)	0.77(7)	1
F2	8	0.2462(8)	0.2462(8)	0.3673(2)	1.41(6)	1

The above variation in lattice parameters with the insertion/deinsertion of sodium into/from the host material can be validated and explained with the help of DFT results. As tabulated in Table 1, the calculated lattice parameters predict the reduction of the a lattice and the increase of the c lattice upon desodiation. The underestimation of the c lattice is observed, which may be due to a slight off-stoichiometry of Na content and Na ion disordering in the layer that may be present in the experimental sample. Nevertheless, tendency of change in lattice parameters with desodiation from $x = 3$ to $x = 1$ is in good agreement with our *ex situ* XRD results. The structural evolution may be explained by considering the charge redistribution in vanadium ions and anions with

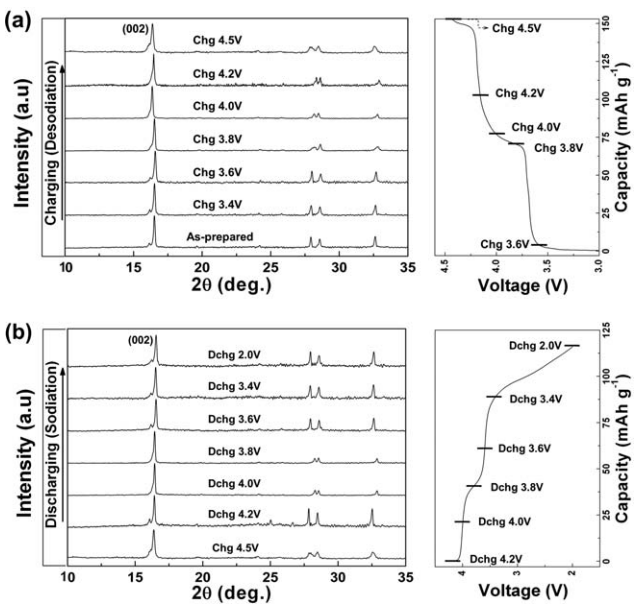

Fig. 3 *Ex situ* analysis of $Na_3V_2(PO_4)_2F_3$ electrodes during (a) charge and (b) discharge. Note that an XRD pattern of an as-prepared electrode in this figure exhibits a considerably different intensity ratio compared to that of as-synthesized powder (Fig. 2a). The main peak at ~16° or (002) peak overwhelms other main peaks at ~28° in the as-prepared electrode, whereas all main peaks have comparable intensities in the as-synthesized powder. We believe that a rolling process in the electrode fabrication caused the preferred orientation of (002).

Table 3 Variation of lattice parameters upon cycling from the *ex situ* XRD data

Voltage	*a* (Å)	*c* (Å)	*V* (Å^3)
As-prepared electrode	9.038(8)	10.73(2)	876.2(8)
3.4[a] V	9.018(9)	10.74(2)	873.2(8)
3.6[a] V	9.007(9)	10.75(3)	872.0(9)
3.8[a] V	8.968(7)	10.76(2)	865.2(8)
4.0[a] V	8.957(8)	10.77(2)	863.9(9)
4.2[a] V	8.948(8)	10.78(3)	863.5(8)
4.5[a] V	8.927(9)	10.80(3)	860.8(9)
4.2[b] V	8.928(8)	10.79(4)	859.7(8)
4.0[b] V	8.928(8)	10.79(3)	859.7(9)
3.8[b] V	8.937(7)	10.78(4)	860.9(7)
3.6[b] V	8.950(8)	10.77(3)	862.6(8)
3.4[b] V	8.971(9)	10.76(3)	866.0(9)
2.0[b] V	9.029(8)	10.74(2)	875.6(8)

[a] Charged state. [b] Discharged state.

desodiation. When Na ions are extracted, V ions are oxidized resulting in the contraction of VO_4F_2 octahedrons. The average distance between neighboring oxygen ions in VO_4F_2 octahedra parallel to the *ab* plane noticeably decreases from 2.801 Å to 2.699 Å as obtained from the DFT calculations. The reduction of the size of VO_4F_2 octahedra, therefore, is attributed to the decrease of *a* lattice. However, in spite of the contraction of VO_4F_2, the *c* lattice parameter increases. This is because the thickness of the Na layer substantially increases as Na ions are extracted. The increased electrostatic repulsions between anions (*i.e.*, F–F and O–O) in the absence of Na ions in the layer significantly expand the Na layer. The distance of F–F in the Na layer along the *c* axis increases from 2.667 Å to 3.216 Å. This large expansion along the *c*-direction dominates over the contraction of VO_4F_2, thus the *c* lattice parameter slightly increases. It is worthwhile noting that the reduction of the *a* lattice and the expansion of the *c* lattice are similarly observed in layered type lithium transition metal oxides in the early stage of delithiation.[40]

The thermal stability of the chemically desodiated phase, $NaV_2(PO_4)_2F_3$, was further investigated at an elevated temperature, as shown in Fig. 4. It can be noticed that the desodiated phase is quite stable up to 550 °C with only 5% weight loss. The initial loss may be due to evaporation of residual acetonitrile used in the chemical desodiation process and/or moisture. The stability of the charged phase implies the feasibility of $Na_3V_2(PO_4)_2F_3$ as a safe electrode material for Na rechargeable batteries.

Electrochemical properties

Fig. 5a shows electrochemical profiles of the $Na_3V_2(PO_4)_2F_3$ cathode in a Na rechargeable battery for selected cycles. The charge/discharge profiles show that there are two plateaus with average voltages of about 3.7 V and 4.2 V. The average voltage of $Na_xV_2(PO_4)_2F_3$ (~3.95 V) is one of the highest among cathode materials with the same redox couple V^{3+}/V^{4+}. The average voltage of vanadium oxides such as V_2O_5 and LiV_3O_8 (*vs.* Li^+/Li^0) ranges from 2.7 V to 3.5 V.[10] Those of NASICON such as $Li_{2-x}NaV_2(PO_4)_3$ and $Li_{1-x}Na_2FeV(PO_4)_3$ are about 3.8 V with V^{3+}/V^{4+} redox couple in lithium cells.[41] Moreover, it is higher than that of $Na_3(VO)_2(PO_4)_2F$ with V^{4+}/V^{5+} redox couple even though the crystal structure of $Na_3(VO)_2(PO_4)_2F$ is very similar to $Na_xV_2(PO_4)_2F_3$.[19] The high potential of V^{3+}/V^{4+} in this

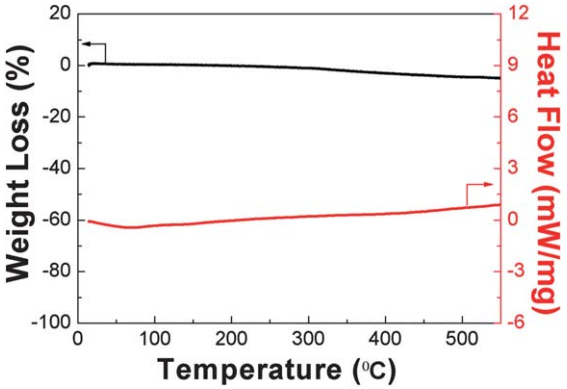

Fig. 4 TGA/DTA analysis of chemically desodiated $NaV_2(PO_4)_2F_3$ at a heating rate of 10 °C min^{-1} in nitrogen.

material is believed to originate from the stronger inductive effects of anion groups. Stronger inductive effects of a fluorine ion as well as a phosphorus ion than oxygen substantially shift up the equilibrium potential of the V^{3+}/V^{4+} redox couple.[8] The high voltage results in a higher energy density of the electrode and is beneficial for practical purposes especially when the Na-ion cell is generally disadvantageous over the Li-ion cell due to lower voltage.[42] The high voltage battery performance is stable for extended cycles as shown in Fig. 5b.

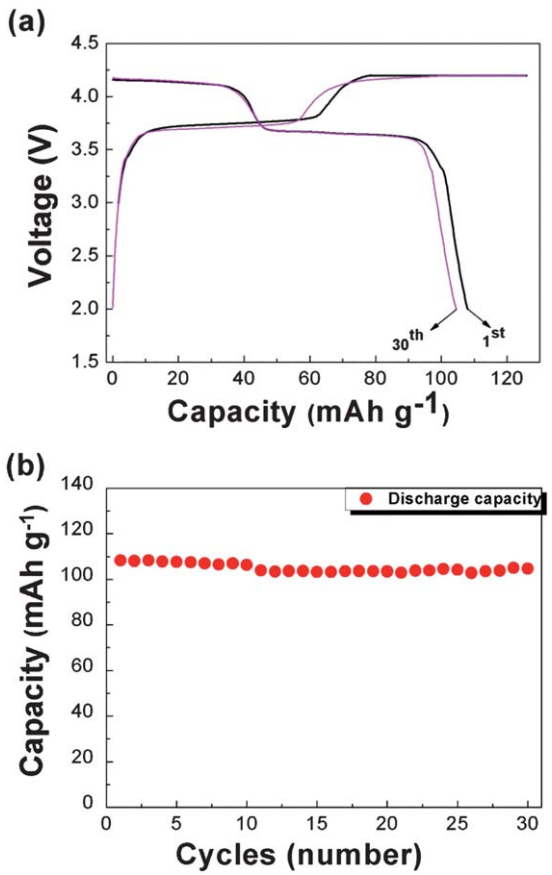

Fig. 5 Electrochemical performance of $Na_3V_2(PO_4)_2F_3$. (a) Charge/discharge profile at the first cycle and thirtieth cycle and (b) cycle performance under a *C*/10 rate.

A first-principles investigation was performed to understand the electrochemical property of $Na_xV_2(PO_4)_2F_3$. The average voltage $\langle V \rangle$ of $Na_xV_2(PO_4)_2F_3$ at $1 \leq x \leq 3$ can be simply determined by using the following equation:

$$\langle V \rangle = -[E(Na_3V_2(PO_4)_2F_3) - E(NaV_2(PO_4)_2F_3) - 2E(Na)]/2F$$

where $E(Na)$ is the energy of elemental sodium in a bcc crystal structure and F is the Faraday constant.[28] The calculated average voltage (*vs.* Na^+/Na^0) is 3.81 V between $x = 3$ and $x = 1$ and is comparable to the experimental observation. In order to elucidate the redox reaction of $Na_xV_2(PO_4)_2F_3$ at $1 \leq x \leq 3$, the valence state of the transition metal is calculated with the removal of the Na ion. The oxidation state of a vanadium ion can be determined by integrating electron spin around the vanadium atom.[32,43] Fig. 6 plots the net spin moment integrated as a function of the distance from the ion core for $Na_3V_2(PO_4)_2F_3$ and $NaV_2(PO_4)_2F_3$. The net spin moments converged into 2 for $Na_3V_2(PO_4)_2F_3$ and 1 for $NaV_2(PO_4)_2F_3$, respectively, around 1.5 Å from the ion core. These values are in agreement with the expected electron spin count of the 3d band of vanadium ions (*i.e.*, 2 for V^{3+} and 1 for V^{4+}), as shown in Fig. 6. This indicates that the electrochemical activity of $Na_xV_2(PO_4)_2F_3$ at $1 \leq x \leq 3$ is mainly attributed to V^{3+}/V^{4+} redox reaction.

It is notable that in spite of the identical redox reaction of V^{3+}/V^{4+} for the compositional range of $1 \leq x \leq 3$ in $Na_xV_2(PO_4)_2F_3$, the difference of the voltage between two plateaus is as much 0.4–0.5 V. It implies that two different environments for Na ions may exist in the material. Even though three Na ions are present at crystallographically equivalent sites in $Na_3V_2(PO_4)_2F_3$, Na ions at Na2 sites are less stable than at Na1 sites because Na ions at the Na2 sites are far shifted from the stable position, as shown in Fig. 1b and d. Therefore, Na ions at Na2 sites have higher chemical potential than those at Na1 sites. As a result, Na ions at Na2 sites are extracted (or inserted) at an earlier stage of charge (or later stage of discharge). After one Na ion is extracted from these sites, it is expected that Na ions will be reorganized to a stable configuration in $Na_2V_2(PO_4)_2F_3$. This is because the configurations with Na in both Na1 sites become comparatively unstable due to short Na–Na distances (2.92 Å).

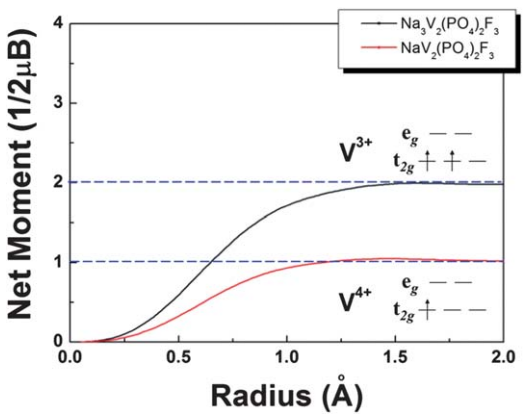

Fig. 6 Integrated spin as a function of integration radius around vanadium ions for $Na_xV_2(PO_4)_2F_3$ at $x = 3$ and $x = 1$. Schematic energy levels and occupied electrons of the 3d bands of vanadium ions of V^{3+} and V^{4+} are presented.

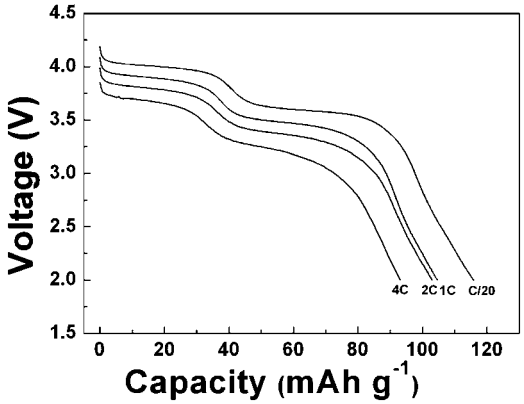

Fig. 7 The rate capability data of $Na_3V_2(PO_4)_2F_3$.

Once the reorganization of Na ions occurs with the increase of distance between Na ions, Na ions are extracted at higher potential due to stabilization, leading to the second plateaus at higher voltages of the profile. This speculation could be verified by first principles calculations of the chemical potentials of Na ions in $Na_xV_2(PO_4)_2F_3$ at $x = 3$ and $x = 2$. In the case of $Na_2V_2(PO_4)_2F_3$, reorganization of Na ions in the Na sites was allowed and various configurations were considered. The most stable Na configuration of $Na_2V_2(PO_4)_2F_3$ among them is shown in Fig. 1e. The chemical potential of a Na ion of $Na_2V_2(PO_4)_2F_3$ (−5.794 eV) is observed to be 0.28 eV lower than that of $Na_3V_2(PO_4)_2F_3$ (−5.514 eV). The difference in the chemical potentials of Na ions is comparable to the voltage difference of the two plateaus of $Na_xV_2(PO_4)_2F_3$ ($1 \leq x \leq 3$) during charge/discharge.

Respectably high rate capability could be obtained from the $Na_3V_2(PO_4)_2F_3$ electrode in a sodium cell as shown in Fig 7. The electrode is capable of delivering a capacity of 120 mA h g^{-1} at the *C*/20 rate and a capacity of 94 mA h g^{-1} even at 80 times higher current density (4*C*) which is about 80% of the capacity at the *C*/20 rate. It should be noted that the average particle size of the as-synthesized powder before the carbon coating process was 1–3 μm (see the ESI†) which is considerably larger than other phosphate based cathodes that show high power.[44–46] The promising electrochemical properties (charge/discharge capacity, cyclability and rate capability) of $Na_3V_2(PO_4)_2F_3$ in a sodium cell can be attributed to low volume change and distortion of the crystal lattice upon charging/discharging which facilitates the fast diffusion of Na ions.

Conclusion

The structural evaluation and electrochemical properties of $Na_3V_2(PO_4)_2F_3$ were studied in a sodium cell through combined computation and experiments. Structural analysis indicates that the reversible sodiation/desodiation occurs *via* one-phase reaction with the negligible variation in lattice parameters (~1%) and cell volume (~2%). An electrochemical study reveals that $Na_3V_2(PO_4)_2F_3$ demonstrates promising charge/discharge, good cyclability, high redox potential and rate capability in Na rechargeable batteries. Further optimization of the $Na_3V_2(PO_4)_2F_3$ electrode can bring Na rechargeable battery sufficiently comparable Li rechargeable batteries.

Notes and references

1 M. Armand and J. M. Tarascon, *Nature*, 2008, **451**, 652–657.
2 B. L. Ellis, W. R. M. Makahnouk, W. N. Rowan-Weetaluktuk, D. H. Ryan and L. F. Nazar, *Chem. Mater.*, 2009, **22**, 1059–1070.
3 S.-W. Kim, D.-H. Seo, X. Ma, G. Ceder and K. Kang, *Adv. Energy Mater.*, 2012, **2**, 710–721.
4 B. L. Ellis, W. R. M. Makahnouk, Y. Makimura, K. Toghill and L. F. Nazar, *Nat. Mater.*, 2007, **6**, 749–753.
5 D. Aurbach, Z. Lu, A. Schechter, Y. Gofer, H. Gizbar, R. Turgeman, Y. Cohen, M. Moshkovich and E. Levi, *Nature*, 2000, **407**, 724–727.
6 R. Berthelot, D. Carlier and C. Delmas, *Nat. Mater.*, 2011, **10**, 74–80.
7 N. Yabuuchi, M. Kajiyama, J. Iwatate, H. Nishikawa, S. Hitomi, R. Okuyama, R. Usui, Y. Yamada and S. Komaba, *Nat. Mater.*, 2012, advance online publication.
8 H. Zhuo, X. Wang, A. Tang, Z. Liu, S. Gamboa and P. J. Sebastian, *J. Power Sources*, 2006, **160**, 698–703.
9 S. P. Ong, V. L. Chevrier, G. Hautier, A. Jain, C. Moore, S. Kim, X. Ma and G. Ceder, *Energy Environ. Sci.*, 2011, **4**, 3680–3688.
10 J. M. Tarascon and M. Armand, *Nature*, 2001, **414**, 359–367.
11 K. Kang, Y. S. Meng, J. Breger, C. P. Grey and G. Ceder, *Science*, 2006, **311**, 977–980.
12 N. Recham, J. N. Chotard, L. Dupont, C. Delacourt, W. Walker, M. Armand and J. M. Tarascon, *Nat. Mater.*, 2010, **9**, 68–74.
13 Y. J. Lee, H. Yi, W.-J. Kim, K. Kang, D. S. Yun, M. S. Strano, G. Ceder and A. M. Belcher, *Science*, 2009, **324**, 1051–1055.
14 J. Barker, M. Y. Saidi and J. L. Swoyer, *Electrochem. Solid-State Lett.*, 2003, **6**, A53–A55.
15 J. Barker, M. Y. Saidi and J. L. Swoyer, *J. Electrochem. Soc.*, 2003, **150**, A1394–A1398.
16 J. Barker, M. Y. Saidi and J. L. Swoyer, *J. Electrochem. Soc.*, 2004, **151**, A1670–A1677.
17 R. K. B. Gover, A. Bryan, P. Burns and J. Barker, *Solid State Ionics*, 2006, **177**, 1495–1500.
18 J. Barker, R. K. B. Gover, P. Burns and A. J. Bryan, *Electrochem. Solid-State Lett.*, 2006, **9**, A190–A192.
19 F. Sauvage, E. Quarez, J. M. Tarascon and E. Baudrin, *Solid State Sci.*, 2006, **8**, 1215–1221.
20 W. Massa, O. V. Yakubovich and O. V. Dimitrova, *Solid State Sci.*, 2002, **4**, 495–501.
21 T. Jiang, G. Chen, A. Li, C. Wang and Y. Wei, *J. AlloysCompd.*, 2009, **478**, 604–607.
22 J. M. Le Meins, M. P. Crosnier-Lopez, A. Hemon-Ribaud and G. Courbion, *J. Solid State Chem.*, 1999, **148**, 260–277.
23 J. Rodríguez-Carvajal, *Newsletter of the Powder Diffraction Commission of the International Union of Crystallography*, 2001, vol. 26, pp. 12–19, available at URL, http://www.ill.eu/sites/fullprof/.
24 J. P. Perdew, K. Burke and M. Ernzerhof, *Phys. Rev. Lett.*, 1996, **77**, 3865–3868.
25 G. Kresse and J. Furthmuller, *Comput. Mater. Sci.*, 1996, **6**, 15–50.
26 G. Ceder, Y. M. Chiang, D. R. Sadoway, M. K. Aydinol, Y. I. Jang and B. Huang, *Nature*, 1998, **392**, 694–696.
27 F. Zhou, M. Cococcioni, C. A. Marianetti, D. Morgan and G. Ceder, *Phys. Rev. B: Condens. Matter Mater. Phys.*, 2004, **70**, 235121.
28 K. Kang, C. H. Chen, B. J. Hwang and G. Ceder, *Chem. Mater.*, 2004, **16**, 2685–2690.
29 F. Zhou, K. Kang, T. Maxisch, G. Ceder and D. Morgan, *Solid State Commun.*, 2004, **132**, 181–186.
30 K. Kang and G. Ceder, *Phys. Rev. B: Condens. Matter Mater. Phys.*, 2006, **74**, 094105.
31 K. Kang, D. Morgan and G. Ceder, *Phys. Rev. B: Condens. Matter Mater. Phys.*, 2009, **79**, 014305.
32 H. Gwon, D.-H. Seo, S. W. Kim, J. Kim and K. Kang, *Adv. Funct. Mater.*, 2009, **19**, 3285–3292.
33 D.-H. Seo, H. Gwon, S.-W. Kim, J. Kim and K. Kang, *Chem. Mater.*, 2010, **22**, 518–523.
34 D.-H. Seo, H. Kim, H. Kim, W. A. Goddard and K. Kang, *Energy Environ. Sci.*, 2011.
35 D.-H. Seo, Y.-U. Park, S.-W. Kim, I. Park, R. A. Shakoor and K. Kang, *Phys. Rev. B: Condens. Matter Mater. Phys.*, 2011, **83**, 205127.
36 D.-H. Seo, H. Kim, I. Park, J. Hong and K. Kang, *Phys. Rev. B: Condens. Matter Mater. Phys.*, 2011, **84**, 220106.
37 V. I. Anisimov, F. Aryasetiawan and A. I. Lichtenstein, *J. Phys.: Condens. Matter*, 1997, **9**, 767–808.
38 A. A. Tsirlin, R. Nath, A. M. Abakumov, Y. Furukawa, D. C. Johnston, M. Hemmida, H. A. Krug von Nidda, A. Loidl, C. Geibel and H. Rosner, *Phys. Rev. B: Condens. Matter Mater. Phys.*, 2011, **84**, 014429.
39 H. Berg and J. O. Thomas, *Solid State Ionics*, 1999, **126**, 227–234.
40 J. Choi and A. Manthiram, *J. Electrochem. Soc.*, 2005, **152**, A1714–A1718.
41 A. K. Padhi, K. S. Nanjundaswamy and J. B. Goodenough, *J. Electrochem. Soc.*, 1997, **144**, 1188–1194.
42 M. Ramzan, S. Lebegue and R. Ahuja, *Appl. Phys. Lett.*, 2009, **94**, 151904–151903.
43 B. J. Hwang, Y. W. Tsai, D. Carlier and G. Ceder, *Chem. Mater.*, 2003, **15**, 3676–3682.
44 J. Kim, Y.-U. Park, D.-H. Seo, J. Kim, S.-W. Kim and K. Kang, *J. Electrochem. Soc.*, 2011, **158**, A250–A254.
45 J. Kim, D.-H. Seo, S.-W. Kim, Y.-U. Park and K. Kang, *Chem. Commun.*, 2010, **46**, 1305–1307.
46 Y.-U. Park, J. Kim, H. Gwon, D.-H. Seo, S.-W. Kim and K. Kang, *Chem. Mater.*, 2010, **22**, 2573–2581.